Lateral diapiric emplacement of Triassic evaporites at the southern margin of the Guadalquivir Basin, Spain

X. BERÁSTEGUI[1], C.J. BANKS[2], C. PUIG[1], C. TABERNER[3], D. WALTHAM[2] & M. FERNÀNDEZ[3]

[1]*Servei Geològic de Catalunya, ICC, Parc Montjuic, 08038-Barcelona, Spain*

[2]*Department of Geology, Royal Holloway University of London, Egham, Surrey, TW20 0EX, UK*

[3]*Institute of Earth Sciences (J. Almera), CSIC, Lluís Solé Sabarís s/n, 08028-Barcelona, Spain*

Abstract: The Guadalquivir Basin is the Neogene foreland basin of the central and western Betic thrust belt in southern Spain. At the boundary between the basin and the outcrops of thrust nappes of Mesozoic limestones of the Prebetic and Subbetic is a broad belt of outcrops of Triassic evaporitic sediments with scattered younger rocks: the so-called 'Olistostrome' unit. This is highly deformed, in places chaotic, and its mode of emplacement has been attributed by various authors to olistostromal debris flow, diapirism, or tectonic melange. Studies of outcrop data in conjunction with seismic and well data, integrated using restorable cross-sections lead us to propose the following sequence of emplacement mechanisms. (a) Loading above a Triassic evaporite formation, probably in the Intermediate Units depositional zone, by north vergent thrusting of thick nappes of Mesozoic sediments, causes northward expulsion of evaporitic sediments between a basal thrust and the base of the limestones. (b) Continued thrust loading drives the diapiric body forwards ahead of the thrust belt, into the floor of the deepening Miocene foreland basin. The body includes blocks of Triassic rocks in normal stratigraphic sequence, as well as blocks of younger rocks broken off the leading hanging-wall cutoffs of the nappes. (c) When the diapiric body reaches the sea-floor of the basin, its top becomes subject to modification by sedimentary processes such as dissolution of evaporites leaving a cap rock and debris flow, both submarine and subaerial but rarely, if ever, forming true olistostromes. (d) At the leading edge of the diapir, northward compression of Miocene basin sediments results in thin-skinned thrusting within these sediments, and formation of duplex structures with a north-dipping monoclinal deformation front. Results from analogue and numerical modelling match the main geological features observed in the study area, thus supporting the plausibilty of the proposed lateral diapiric emplacement of the chaotic unit.

Between the frontal thrust zone of the central and western Betics and the Guadalquivir foreland basin (Fig. 1) there is a unit characterized by outcrops of chaotic Triassic gypsum and folded red-bed clastics, with some scattered younger blocks, mostly of Upper Cretaceous limestones. These outcrops have been referred to as 'Olistostromic Zone' by Perconig (1960–62), and many authors have followed his nomenclature and interpreted this unit as a sedimentary melange or olistostrome (Pérez-López & Sanz de Galdeano 1994). Alternative names used are 'Guadalquivir Allochthonous Unit' (Blankenship 1990, 1992), and by our group informally 'SCO' standing for 'So-Called Olistostrome' (chaotic unit). In fact, the most recently published geological maps are based on the olistostrome model, where Tertiary formations have been interpreted as the matrix supporting blocks of gypsum and other rocks.

The unit made up mainly of chaotic Triassic sediments at the front of the thrust belt is a very unusual aspect when compared with 'classical' thrust fronts. It is generally agreed that the unit is derived from the thrust belt, but its composition, geometry, exact origin and mode of emplacement are all contentious.

The aim of this paper is to interpret the mechanism of emplacement of the chaotic allochtonous unit and its geodynamic relationships with both the thrust belt and the foreland basin. Seismic reflection, oil wells and field geological data including those from recent (1980s) oil and gas exploration surveys and exposures from road building have been used in refining the stratigraphical and structural interpretation of the study area. The application of sequence-stratigraphic methodology to the basin-fill has permitted us to time the emplacement of the chaotic unit. The new information presented

BERÁSTEGUI, X., BANKS, C. J., PUIG, C., TABERNER, C., WALTHAM, D. & FERNÀNDEZ, M. 1998. Lateral diapiric emplacement of Triassic evaporites at the southern margin of the Guadalquivir Basin, Spain. *In:* MASCLE, A., PUIGDEFÀBREGAS, C., LUTERBACHER, H. P. & FERNÀNDEZ, M. (eds) *Cenozoic Foreland Basins of Western Europe*. Geological Society Special Publications, **134**, 49–68.

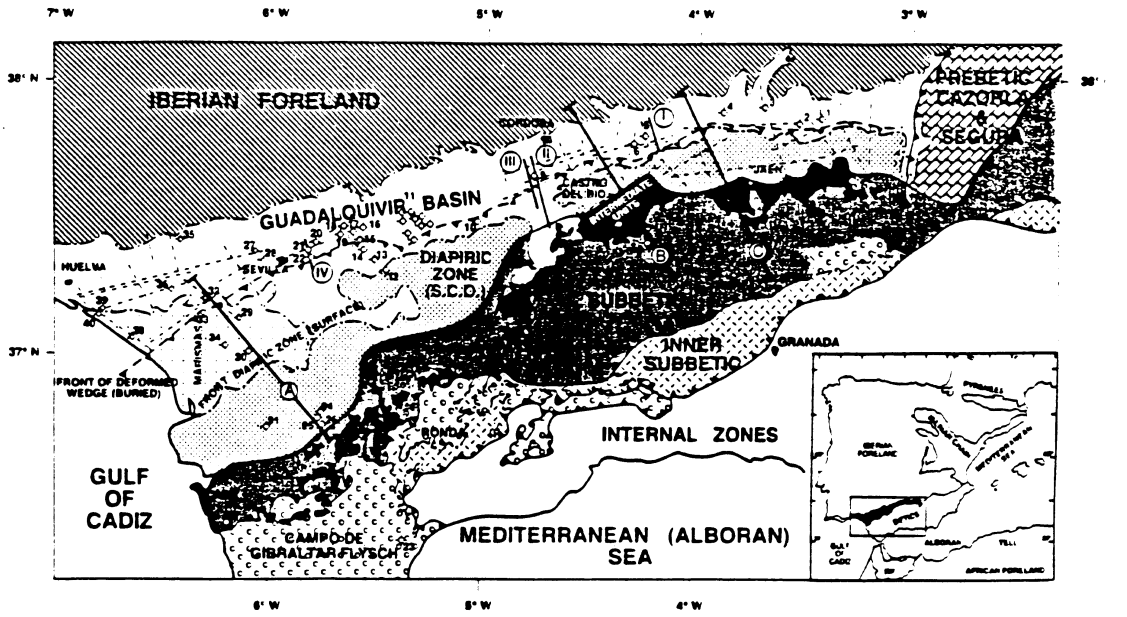

Fig. 1. Structural map of the central and western Betics and Guadalquivir Basin and location map of oil-wells, seismic profiles and cross-sections. Cross-sections: A, Marismas section (Fig. 4); B, Baena section (Fig. 3); C, Martos section (Figs 2 and 5). Seismic profiles: I (Fig. 9); II (Fig. 6); III (Fig. 7); IV (Fig. 10); broken lines correspond to different profiles used in the interpretation. Well number: 1, Baeza-1; 2, Baeza-2; 3, Baeza-4 or Bailén; 4, Villanueva de la Reina or Baeza-3; 5, Rio Guadalquivir K-1; 6, Bujalance; 7, Rio Guadalquivir H-1; 8, Nueva Carteya-1; 9, Rio Guadalquivir N-1; 10, Ecija 1 and 2; 11, Córdoba A-1 to A-7, Córdoba B-1 and B-2, and Córdoba C-1; 12, Carmona 6; 13, Carmona-5; 14, Carmona-4; 15, Carmona-3; 16, Carmona-2; 17, Sevilla-3; 18, Carmona-1; 19, Sevilla-1; 20, Ciervo; 21, Sevilla-2; 22, Sevilla-4; 23, Cerro Gordo-3; 24, Bornos-3; 25, Bornos-1; 26, Angostura-Bornos; 27, Salteras-1; 28, Castilleja; 29, Isla Mayor, 30, Bética 14-1; 31, Bética 18-1; 32, Villamanrique; 33, Casanieves; 34, Sapo-1; 35, Villalba del Alcor-1; 36, Almonte-1; 37, Chiclana; 38, Asperillo; 39, Huelva-1; 40, Moguer-1. Guadalquivir Basin: in white, Miocene to Quaternary; in dots, marine Pliocene to Quaternary (Marismas area).

here on the structure of the External Betics, and the Guadalquivir Basin enables us to propose a diapiric hypothesis for the emplacement of the chaotic unit. Restorable geological cross sections and numerical and physical (sand-box) modelling have been applied to test the reliability of the proposed geodynamic hypothesis.

Geological setting

The Guadalquivir Basin is the Neogene foreland basin of the central and western half of the Betic Cordillera (Fig. 1). At its eastern termination it is bounded by the NNE-striking thrust imbricates of the Cazorla Zone and the big thrust anticlines of the Sierra de Segura. The eastern half of the Cordillera has no foreland basin because deformation of the thick sedimentary cover extends far beyond the limits of load-induced flexural subsidence of the basement. East of Córdoba the Guadalquivir Basin is very narrow and shallow, but it widens and deepens to the west. The basin floor dips fairly uniformly at a shallow angle to the SSE, with basement (Hercynian Iberian Massif) emerging at a remarkably straight but unfaulted basin boundary to the NNW.

The Betic Cordillera comprises the Internal and External Zones. The Internal Zones consist of metamorphic basement and Palaeozoic–Triassic sediments of varying metamorphic grade in big domal culminations elongated more-or-less E–W, including some outcrops of peridotites in the Ronda area. The emplacement of the dense rocks of the Internal Zones onto the former passive margin of southern Iberia was responsible for both the load-induced subsidence of the margin and the compressive deformation of the Betics (van der Beek & Cloetingh 1992; Banks & Warburton 1991). Any obliquity of transport direction (Leblanc & Olivier 1984; Frizon de Lamotte *et al.* 1991), and any non-compressive deformation, were resolved during deformation of the External Zones (for example by vertical pole rotation of individual thrust slices; Allerton

et al. 1993) so that the only process affecting the thrust front was NNW-directed compression. The first compressive phase that affected the southern margin of the External Zones took place in the Eocene. The main phase of compression was in the Mid-Miocene (Late Langhian–Serravallian), but compression did not finally die out until the Tortonian.

The External Zones

Stratigraphy

The stratigraphy and palaeogeography of the External Zones of the Betic Cordillera have been the subject of many works since the 1920s; key papers are Fontboté (1965); García Hernández *et al.* (1980); Baena & Jerez (1982); Vera *et al.* (1982) and Fontboté & Vera (1984). In summary, the External Zones consist of a tectonically detached cover of Mesozoic sediments ranging from Middle Triassic to Upper Cretaceous–Palaeocene pre-tectonic units, and Eocene to Lower Miocene syn-tectonic deposits. From palaeogeographic and tectonic considerations, the External Zones are divided into Prebetic and Subbetic (Fig. 1). The Prebetic is made up of shallow-marine and continental Mesozoic carbonates and capped by continental Palaeogene sediments. It does not crop out in the central Betics. The Subbetic is characterized by Mesozoic dominance of pelagic facies in the strata of Upper Liassic to Upper Cretaceous–Palaeocene age. From thickness variations and tectonic position, Subbetic is usually divided into Intermediate Units and Subbetic proper. Among the significant characteristics of the Intermediate Units are the thickness of the Mesozoic strata (more than 2000 m of Jurassic and Lower Cretaceous, mostly slope to basinal sediments). Well data show that the Triassic in the Intermediate Units comprises only a thin section of 'Supra-Keuper' dolomites and anhydrites of uncertain Jurassic to Triassic age lying immediately above a regional detachment.

The Mesozoic series in the Subbetic proper are much thinner than in the Intermediate Units, and include radiolarites and ammonitico rosso facies as well as carbonate turbidites at different levels in the Jurassic succession. In places, there are also pillow lavas defining a 'Median Subbetic' unit. The Triassic in the External Subbetic crops out in very extensive areas and has been the subject of many studies, from Blumenthal (1927) to Pérez López (1991). The latter author defined, from bottom to top, the Majanillos Formation (Muschelkalk), Ladinian in age, which consists of dolomites and limestones; the Jaén Group (Keuper), Karnian in age, which consists of multicoloured mudstones including evaporites, carbonates and clastics (K1), red sandstones and mudstones (K2), red mudstones and dolomites ('carniolas', K3) and evaporites (K4–5); and the Ocres Rojos or Zamoranos Formation, Norian in age, consisting of dolomites and limestones.

Structure

Between Córdoba and Granada, structures are well exposed, and seismic and well data are

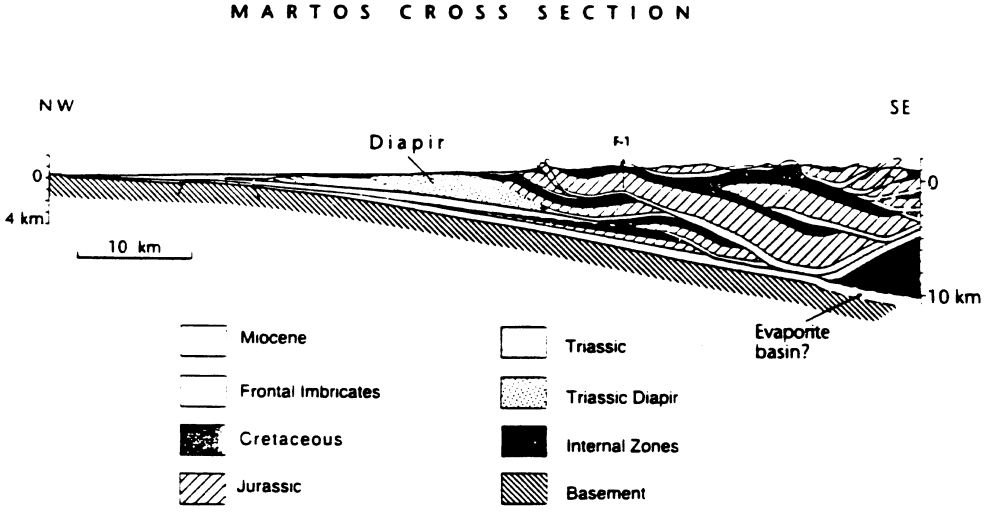

Fig. 2. 'Martos' geological cross-section based on outcrop data, seismic lines RGKO-89-01, 82-31 & 32 and Fuensanta-1 well, and speculative extrapolation.

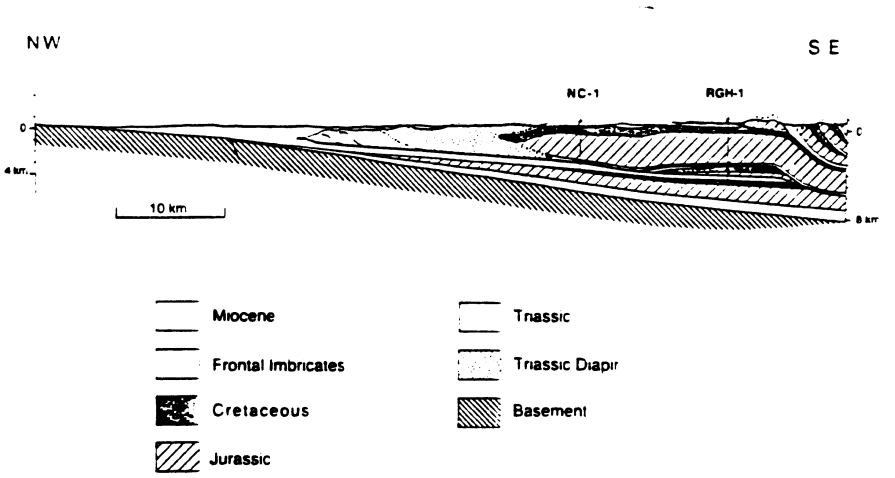

Fig. 3. 'Baena' geological cross-section, based on outcrop data, seismic lines BT-8A, S-83-34, S-84-40, S-83-44 and AES lines, and Nueva Carteya-1 and Rio Guadalquivir H-1 wells. It shows variation of structure about 40 km down strike.

available. The data have been compiled and interpreted using conventional thrust-belt techniques. The three structural cross-sections, 'Martos', 'Baena' and 'Marismas', (see Fig. 1 for location and Figs 2, 3 and 4) are drawn at true scale with the available data accurately placed, and although they are in places unconstrained, and not unique solutions, they are restorable. The only previous attempt to interpret the region using this methodology was by Blankenship (1992). The interpretation proposed in this paper is based in part on the interpretation of the eastern Betics of Banks & Warburton (1991), and involves a relatively large amount of shortening: at least 80 km shortening of the Jurassic on the part of the Betics shown in Fig. 2.

Figure 5 shows an interpretation of the Martos section (see Fig. 1 for location) in terms of the tectonostratigraphic zones discussed above and demonstrates the volumetric importance of the Intermediate Units (proven by the two wells on the Baena section, Fig. 3) and the insignificance of the Prebetic in this area (in this paper we consider the 'Prebetic of Jaén' and similar units as a part of the Intermediate Units). The 'frontal thrust' of the Intermediate Units is in fact a subtractive contact with the chaotic unit. The Subbetic can be deduced to be a duplex, with basal detachment consistently within the Middle Triassic. The frontal Subbetic thrust carries it over the Intermediate Units duplex, in which the basal detachment is in Supra-Keuper and the roof detachment is in the Lower Cretaceous.

The proposed general relationship between the Intermediate Units, the Subbetic proper, and the Internal Zones is best seen on the Martos structural section (Fig. 2). A wedge of Internal Zones basement is driven in at the basal (Triassic) detachment, so that the Subbetic proper is uplifted in a synform. The Subbetic leading edge is thrust over the Intermediate Units in a shallow flat-lying nappe, with windows and klippen, but otherwise the Subbetic proper is mainly internally deformed into a backthrust duplex thrusting top-to-south back onto the Internal Zones (all of the actual displacements, of course, being northwards the Iberian Massif).

The Triassic at the base of the frontal nappe of the Subbetic proper forms extensive areas of outcrop and has obviously moved in part diapirically (Pérez-López & Sanz de Galdeano 1994). For example, in the low area between the Martos and Baena cross-sections, the Triassic appears to overlie completely the Intermediate Units so as to merge with the Triassic of the chaotic unit (whereas the Jurassic limestones, that are carried by it are overturned, suggesting a possible 'tank-track' mode of emplacement). However, the bedded Subbetic Triassic can be distinguished in the field from the Triassic forming the chaotic unit, in that the former contains well-bedded sequences of mudstones to sandstones, with relatively little gypsum. These

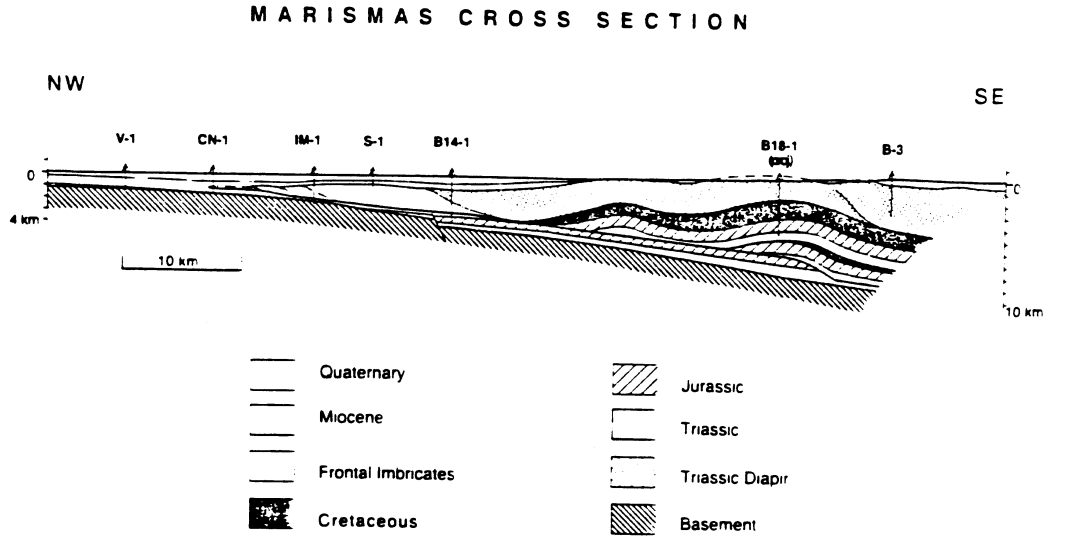

Fig. 4. 'Marismas' geological cross-section, based on a few outcrop data, seismic line MA-3 and others, and 7 wells (V, Villamanrique-1; CN, Casa Nieves-1; IM, Isla Mayor-1; S, Sapo-1; B14-1 and B18-1 are Esso Betica wells; B-3, Bornos-3). In Betica-18-1 the diapir is mostly halite.

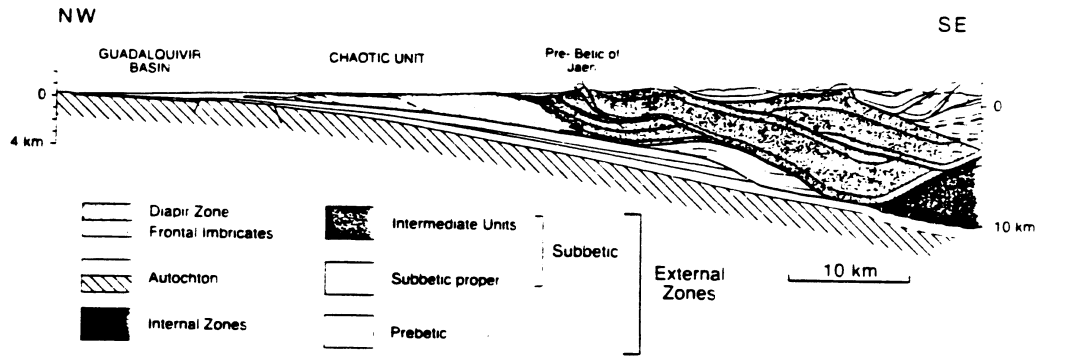

Fig. 5. 'Martos' cross-section displaying the tectonostratigraphic zones. It shows how diapir zone extruded along the base of Intermediate Units. Prebetic of Jaen is represented structurally as a part of Intermediate Units.

bedded outcrops are mainly bright red, as opposed to the very mixed purple-red, green and other colours of the chaotic unit.

In the central Betics, there is some evidence indicated on both cross-sections for deformation below the base of the Intermediate Units thrust sheet, arching it upwards. This must be the youngest thrust deformation, and we consider it to be parautochthonous Prebetic (Fig. 4). In fact, seismic data in the vicinity of well Bética 18-1 show a broad antiformal structure that may indicate a Prebetic structure below the 'chaotic unit'.

Composition and structure of the chaotic unit

The aforementioned 'Martos', 'Baena' and 'Marismas' structural sections (Figs 2, 3 and 4) show how the deeper SE half (or more) of the Guadalquivir foreland basin is occupied by the allochthonous chaotic unit that is the subject of this paper. From seismic and well data (see below), the chaotic unit has two parts. The most external part, which is not exposed, comprises imbricated Miocene sediments of the basin fill. It has a basal thrust in the early Mid-Miocene,

leading to a blind deformation front. Seismic stratigraphy (see also Fernández *et al.* this volume) shows that only the Serravallian and Tortonian are deformed, with the youngest Tortonian, Messinian and Pliocene onlapping the top surface of the deformed Miocene strata, which is an unconformity. In some places there is a possible passive backthrust in the upper part of the deformed unit. The inner part of the chaotic unit appears as a chaotic mass on seismic profiles. Outcrops indicates that it consists of Triassic gypsum and clays with the characteristic colours including purple, red, green and grey, with no coherent bedding or structure at regional scale. This mixture of lithologies encloses blocks, tens to hundreds of metres in size, of various formations including Upper Cretaceous to Palaeocene carbonates (Capas Rojas Formation), Triassic carbonates (Zamoranos and Majanillos Formations) and Triassic basic volcanic rocks (ophites); Jurassic carbonates apparently do not occur as blocks. The contacts, where seen, are typically tectonic or diapiric, with brecciation of the Keuper and the block material extending over a few decimetres. The chaotic unit is typically 2–3 km thick, and 10 km wide in the central Betics. However, further west (see 'Marismas' section, Fig. 4) the width increases to at least 50 km, and the wells show that it includes a significant proportion of halite. In the Montilla area, the top of the chaotic unit is depressed, and seismic shows that this is due to an array of shallow listric normal faults of probably Pliocene age (Fig. 6).

In most of the outcrop area the chaotic unit lies directly below Quaternary soils and fluvial terraces, but in around Castro del Rio it is overlain by Serravallian clastics and marls (turbidites of Castro del Rio area; see also Roldán *et al.* 1992) which very commonly show steep diapiric contacts.

The seismic image of the inner part of the chaotic unit consists of non-coherent reflections (Fig. 6) within a package defined by south-dipping boundaries so that the Intermediate Units overlie the internal edge of the chaotic unit. The external sub-unit is seismically much more coherent than the inner part (see Figs 6 and 7), and consists of sub-parallel sets of reflections displaying fold geometries cut by faults, which make the whole interpretable as a small north-verging imbricated thrust system. The contact between the two parts of the chaotic unit could be either a thrust or a primary diapiric contact (Figs 2, 3, 6 and 7). On the third cross-section, Marismas (Fig. 4), located 160 km further west, the chaotic unit is considerably larger and its limit to the SE is not constrained. The external sub-unit is clearly seen on seismic and in wells: Isla Mayor-1 penetrated the sub-unit completely and showed that it consists in deformed and repeated Miocene. The wells Betica 18-1 and Bornos-3 drilled thick sequences of the internal sub-unit and showed that it consists mainly of halite (north of Jaén, halite is produced commercially by solution from the internal sub-unit).

Since the early works by Perconig (1960–62) the chaotic unit has been interpreted by many authors (e.g. Pérez López 1991; Riaza & Martínez del Olmo 1995) as a chaotic mass formed by a matrix of Triassic sediments and including younger blocks, which flowed into the basin during Tortonian times in the form of gigantic olistostromic masses derived from the Subbetic. Therefore, the chaotic unit has been considered as a mega-turbidite forming a part of the sedimentary infilling of the basin (e.g. Suárez-Alba *et al.* 1989).

However, the term olistostrome denotes 'a sedimentary deposit which consists of a chaotic mass of rock and contains large clasts composed of material older than the enclosing sedimentary sequence. The clasts may be gigantic and are then called "olistoliths". Such deposits are generally formed by gravity sliding of material, sometimes into oceanic trenches. Olistostromes have also been called "sedimentary melanges"' (Allaby & Allaby 1990).

Keuper gypsum, as seen in the outcrops of the chaotic unit, is not a plausible matrix lithology for a deep-water sediment and is different from the observed Triassic of the Subbetic. Furthermore, a Triassic olistostrome matrix cannot enclose younger (Upper Cretaceous) olistoliths. We interpret the subtractive contacts at the front of the Intermediate Units referred to above (Figs 2, 3 and 5) as diapiric contacts, and therefore we propose that the evaporites were derived from below the Intermediate Units, where the Keuper is now absent, and emplaced below the seismically recognized south-dipping tectonic contact. This is a diapiric process.

The Guadalquivir Basin

The basement of the basin consists of Palaeozoic and Mesozoic rocks, its top dipping some 2–4° towards the SE. It holds a Neogene to Quaternary sedimentary infilling, with a major megasequence boundary between them. Previous works focusing on the stratigraphy of the infilling considered it as formed by two different types of deposits, both from lithological and genetic points of view: (1) massive, allochthonous olistostromes dropping into the basin from

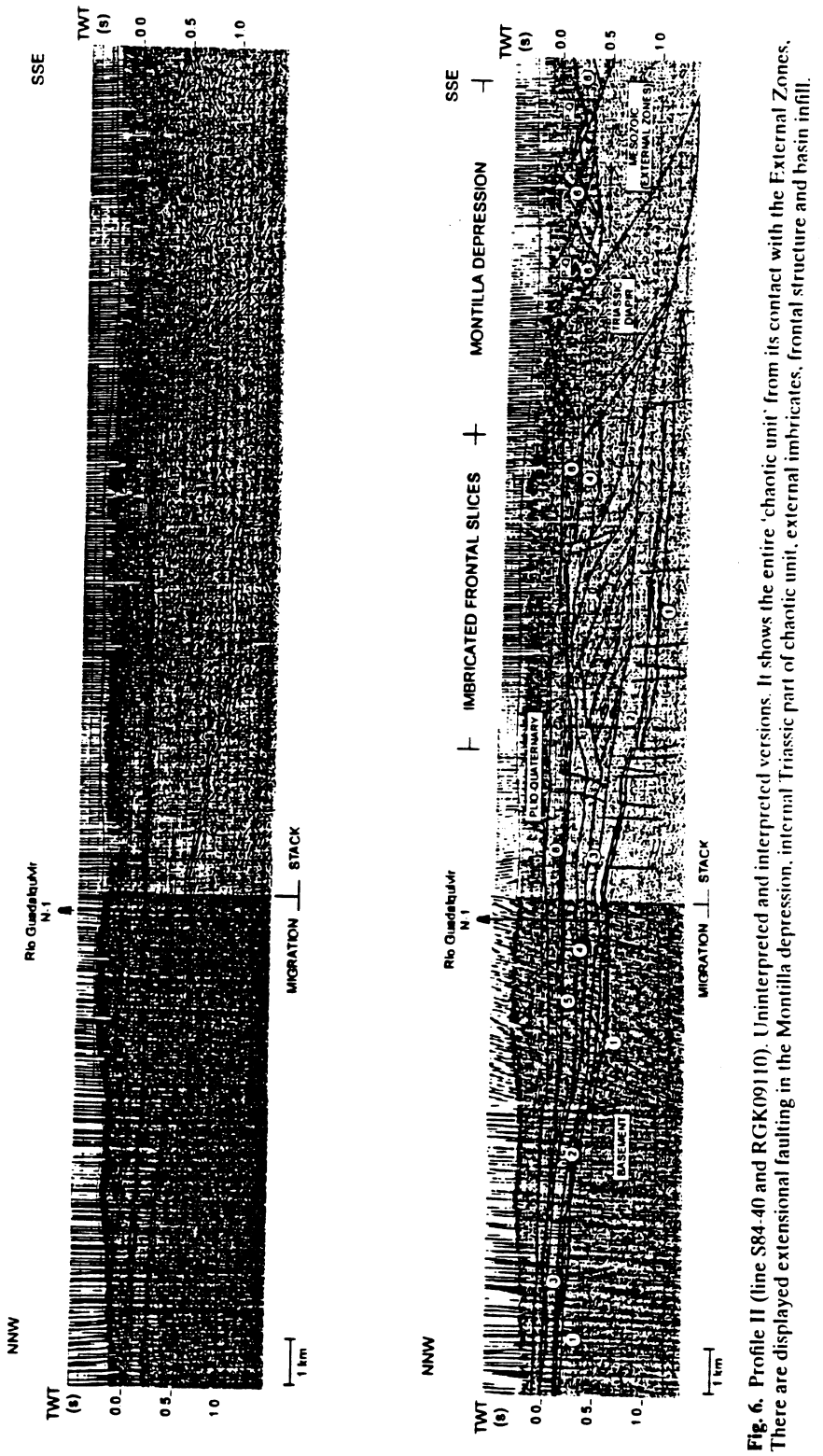

Fig. 6. Profile II (line S84-40 and RGK09110). Uninterpreted and interpreted versions. It shows the entire 'chaotic unit' from its contact with the External Zones. There are displayed extensional faulting in the Montilla depression, internal Triassic part of chaotic unit, external imbricates, frontal structure and basin infill.

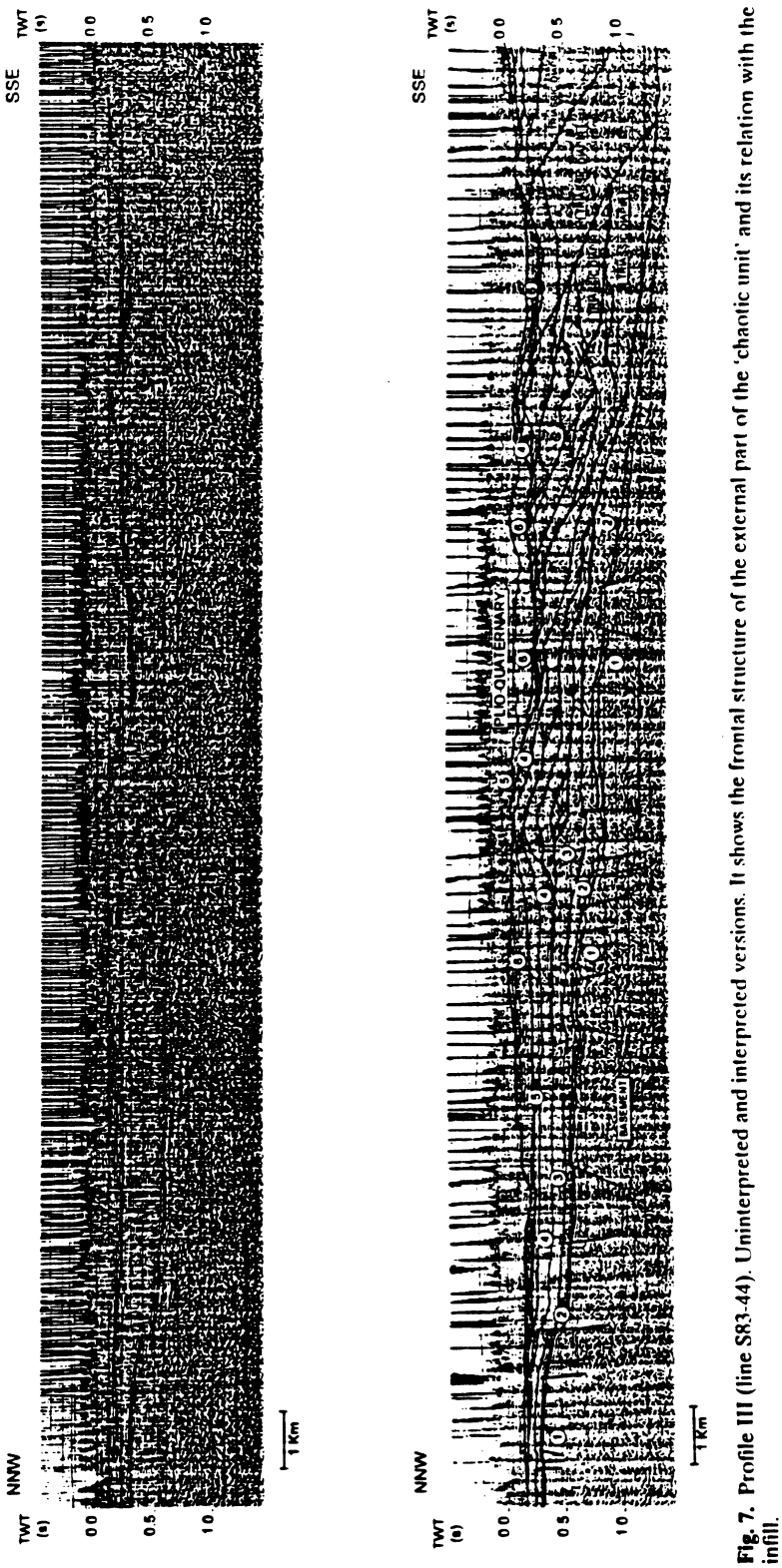

Fig. 7. Profile III (line S83-44). Uninterpreted and interpreted versions. It shows the frontal structure of the external part of the 'chaotic unit' and its relation with the infill.

the External Zones of the chain, and (2) 'autochthonous' sedimentation (see Fernàndez *et al.* this volume).

The interpretation of seismic stratigraphy from more than 1400 km of seismic lines and 35 exploration wells (Lanaja *et al.* 1987; see Fig. 1 for location) has enabled us to divide the Miocene sedimentary infill of the basin into six seismic-stratigraphic, depositional sequences (Mitchum *et al.* 1977; Vail 1987) numbered, from bottom to top, sequences 1 to 6 (Fig. 8). They are widely recognizable in the whole basin. Because of problems in dating the coastal and nearshore sediments forming the sequence 1 in outcrop and in the available wells (see details in Fernández *et al.* this volume), the age attributions have been made using seismic-stratigraphic techniques. Thus, taking as a datum the regionally well-known Late Messinian Unconformity, the defined sequences have been tied to third-order cycles 2.4 (Late Tortonian–Early Serravallian) to 3.3 (Messinian) in supercycles TB2 and TB3 of the Standard Cycle Chart (Haq *et al.* 1987) (Fig. 8). The nature of the boundaries, seismic facies, thicknesses, lithologies and attributed sedimentary environments are summarized in Table 1.

In relation to the extensional faulting involving the basement, sequence 1 clearly predates the extensional structures; the thickness of sequence 2 is controlled by normal fault offsets, showing important N–S variations, increasing towards the internal zones of the basin, and pinching out towards the structural highs of the basement developed in the northern half of the basin (Córdoba area). From outcrop data, sequence 2 can be correlated with the Castro del Rio sands and marls, where it unconformably overlies the Triassic, internal part of the chaotic unit, and is involved in minor diapiric structures. The structural highs also control the arrangement of the sequences 3 and 4 (Figs 9 and 10), which post-date the normal faults.

Sequence 3 is involved in the frontal imbricates, sequences 4 and 5 forming its frontal monocline; also some remains of these sequences can be found on the hanging wall of the structure (Fig. 7). Sequence 6 post-dates all the structural features, and the bottom of the Pliocene deposits, especially in the Córdoba area, is deeply incised in the previous sediments (Fig. 10).

Structural modelling of lateral diapirism

In the last few years, big advances have been made in the understanding of diapiric processes, and their relationship with other structural and stratigraphic processes. The physical modelling work of the Applied Geodynamics Laboratory (AGL) in Austin, Texas, using sand and polymers, has made a particularly important contribution to the understanding of lateral movement of salt in the Gulf of Mexico (Jackson & Talbot 1989). Further advances in this passive continental margin setting have been made using cross-section balancing techniques (McGuinness & Hossack 1993; Hossack 1995). Application of these techniques to seismic data from the Gulf Coast has led to the recognition that major lateral flow of diapiric material often takes place both within sediments as intrusions.

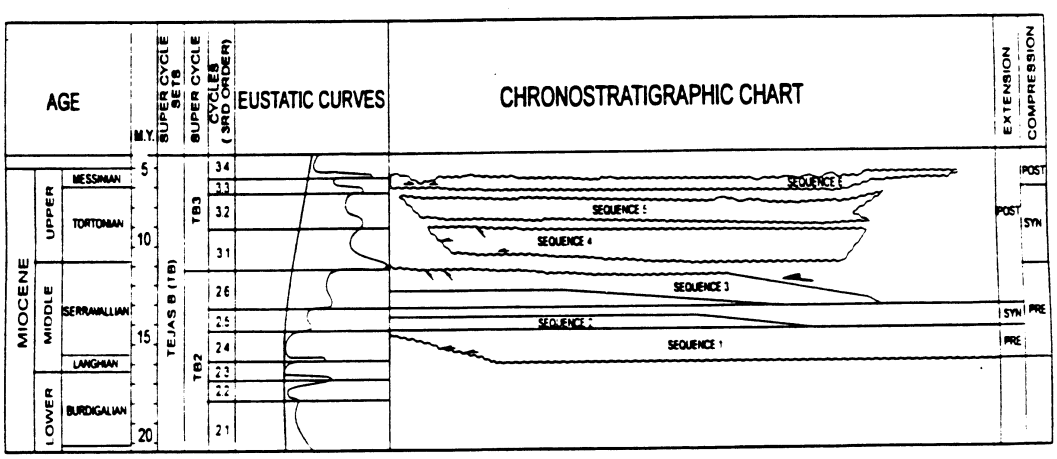

Fig. 8. Cycle chart showing the established sequences and its correlation to the standard cycle chart (Exxon). Also there are two columns in which the sequences are correlated to the basement extension and to the chaotic unit emplacement (compression), pre-syn-post in each.

Table 1. *Summary of the seismic stratigraphic interpretation and correlation with the Standard Cycles of Haq* et al. *(1987)*

This work	Standard cycle chart Haq *et al.* (1987) Supercycles	Ma	Age	Boundaries	Thickness	Lithology	Internal seismic pattern	Depositional environment
6	3.3		Messinian	Lower boundary: erosive unconformity (toplap terminations below it). Very late Tortonian unconformity. Upper boundary: very important erosive surface with deeply incised channels and valleys. Very late Messinian unconformity.	Very irregular in the whole basin. It ranges from 0 to 400 ms (TWT). The higher values are in Marismas area.	Marls and sandy marls with sand intercalations.	Sub-parallel, continuous reflections with areas of strong amplitude (specially near the bottom) and slight amplitude (in the upper half of the section), of low apparent frequency.	Basinal/ turbiditic
		6.3						
5	3.2		Mid- and late Tortonian	Lower boundary: Mid-Tortonian unconformity. Upper boundary: Very late Tortonian unconformity.	From 20 ms to 80 ms (TWT). Its maximum value is 200 ms (TWT) in Córdoba area.	Marls, silts and sands.	Strong amplitude, high frequency and good continuity reflections which show mounted, channelled and progadationals geometries.	Turbiditic
		8.2						
4	3.1		Early Tortonian	Lower boundary: Very late Serravallian unconformity. Upper boundary: erosive unconformity. Mid-Tortonian unconformity.	It is in infilling the erosion features from Tortonian erosive surface. Its thickness is very irregular ranging from 300 ms to 0 ms (TWT).	Sands and marls.	Strong to moderate amplitude, low apparent frequency and good continuity reflections, showing sub-parallel, mounded and channelled geometries in strike sections.	Turbiditic
		10.5						
3	2.6		Late Serravallian	Lower boundary: erosive unconformity (toplap terminations of the sequence 2). Mid-Serravallian unconformity. Upper boundary: very important erosive unconformity defined by toplap reflection terminations. Very late Serravallian unconformity.	From 30 ms to 80 ms (TWT). Its maximum value is 200 ms in Córdoba area.	Marls with sandy intercalations.	Sub-parallel to oblique, apparent low frequency, slight amplitude and poor continuity in the deepest areas.	Basin/ turbiditic
		12.5						
			Early Serravallian	Lower boundary: Onlap surface. Early Servallian	Controlled by normal faults. Its maximum	Marls with intercalations	Low amplitude and apparent poor continuity, sub-parallel reflections	Basin/ turbiditic

2	2.5			unconformity. Upper boundary: unconformity including an erosional toplap below the sequence 3. Mid-Serravallian unconformity.	value is 300 ms (TWT).	of sands.	in the shallower parts of the basin, and high amplitude, low apparent frequency and good continuity, sub-parallel, oblique, mounded and channel-shaped reflections in the deepest areas.	
		13.8						
1	24		Very late Langhian to very early Serravallian	Lower boundary: Very late Langhian unconformity. Upper boundary: Early Serravallian	From 20 to 40 m. The maximum values are found in Sevilla area.	Calcarenites, conglomerates and sandstones.	Not imaged on the available profiles.	Coastal and near shore.
		15.5						

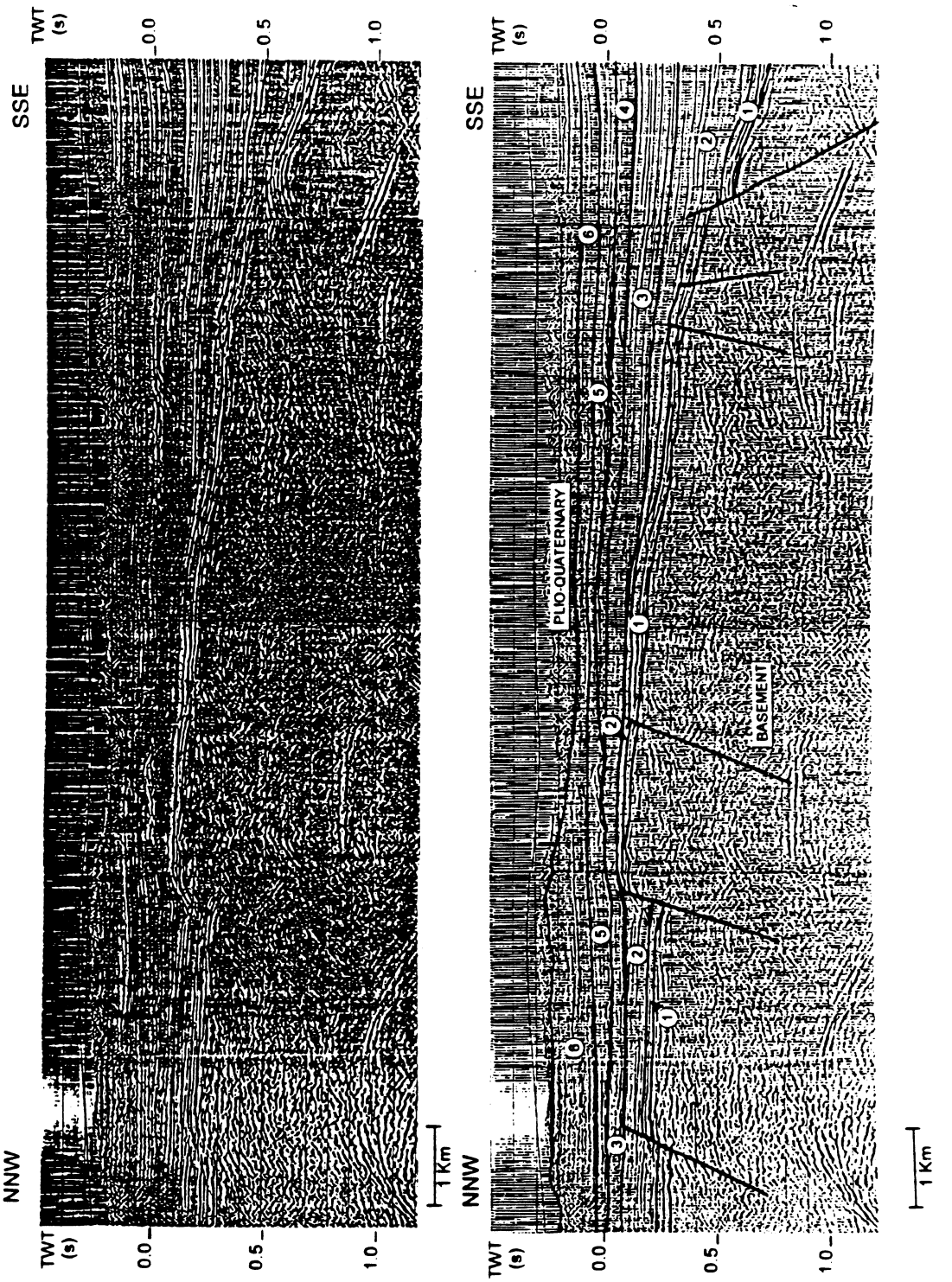
SSE
NNW
TWT (s)
0.0
0.5
1.0
1 Km
PLIO-QUATERNARY
BASEMENT
1
2
3
4
5
6

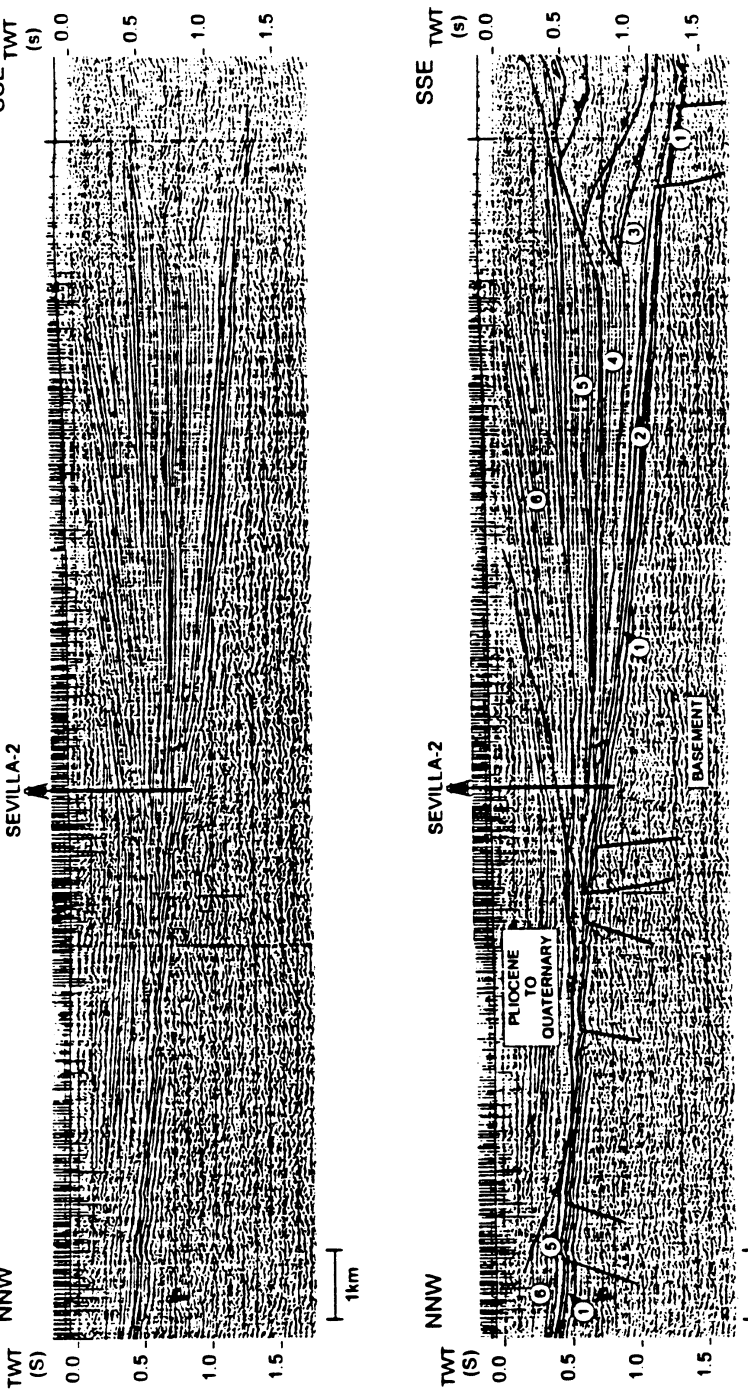

Fig. 10. Profile IV (line 81-58). Uninterpreted and interpreted versions. It shows the pinching out of sequences 2 and younger over the basement highs (Córdoba-Sevilla area). Also shows S-N progradational pattern of Pliocene sequences and paleo-Guadalquivir incision. Includes well Sevilla-2.

and at the sea bed by processes analogous to the flow of glaciers. Salt 'glaciers' have also been studied where diapirs emerge at surface in the semi-arid conditions of the Zagros fold-belt, Iran. Here the term 'namakier' (from the Farsi word for salt, *namak*) has been given to them (Talbot 1981). When they form at sea-bed they partly dissolve, until they acquire a carapace of insoluble residue and marine sediments. So long as the supply of diapiric material from below is sufficient to maintain some surface or seabed topography, the namakier will continue to flow (Fletcher *et al.* 1993).

Analogue sand-box physical model

A provisional attempt was made to model the structure as interpreted on the Martos and Baena cross-sections (Figs 2 and 3), on the assumption that it is a diapiric body emplaced laterally under compression (most of the AGL published models involve extension). The experiment was carried out in the Fault Dynamics Project laboratory at Royal Holloway University of London. Figure 11 shows the starting configuration of the experiment. It includes an unstable asymmetric 'basin' of SGM polymer to simulate the original basin of Keuper evaporite, overlain by a wedge of sand (dark grey and white) thinning towards the foreland, represented by a block of wood with a 25° ramp. The model was tilted about 3°, then compressed from the 'internal' end.

We had expected deformation to start with the formation of an imbricate stack of thrust slices propagating from the moving end wall (right), simulating the Betic thrust belt, but this did not occur. Instead, the sand layers detached as a single block on a thrust that ramped to surface above the basement step. This meant that the tectonic load necessary to drive out the polymer did not develop. At this point we stopped the compression, and introduced an artificial load in the form of metal weights. This made the polymer flow from below the weights and up into a pillow above the basement ramp and into the initially formed thrust. Then the metal weights were removed, and the space filled with light grey and thin white sand layers (which can be regarded as early syn-compressive beds). During subsequent compression, 'pop-up' thrust structures developed in the internal part of the model, but still not a good analogue for the external Betics.

As compression continued, the diapir enlarged, and was pushed by the large block of pre- and syn-tectonic material. Its base moved on a flat thrust over the basal (white) layer of pre-tectonic sediment. At the top of the diapir, the thin pre-tectonic layers soon stretched to negligible thickness, and the polymer emerged, flowing down the slope into the foreland basin and overriding deformed basin-fill sediments (white and thin light grey layers). Polymer also intruded the sand layers on both sides of the diapir.

The final result (Fig. 12) shows striking similarities with the interpreted cross-sections, especially the 'Baena' section, (Fig. 3) although it must be admitted that in this preliminary experiment the procedure was somewhat contrived. Figure 13 shows a schematic model for the emplacement of the diapiric body into the southern margin of the Guadalquivir Basin, showing also how blocks of younger limestones can be broken off the tip of the overthrusting Jaen Zone and incorporated into the diapir.

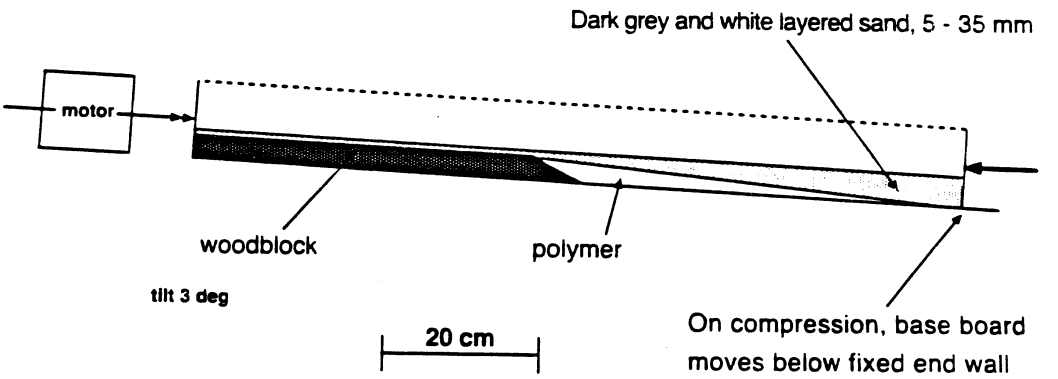

Fig. 11. Model set-up for sandbox experiment. The box measures 100 cm long, 30 cm wide, 10 cm deep. On compression, the base-board moves below the fixed end-wall at the right. This means that deformation starts at this end (internal) and propagates to the left (external).

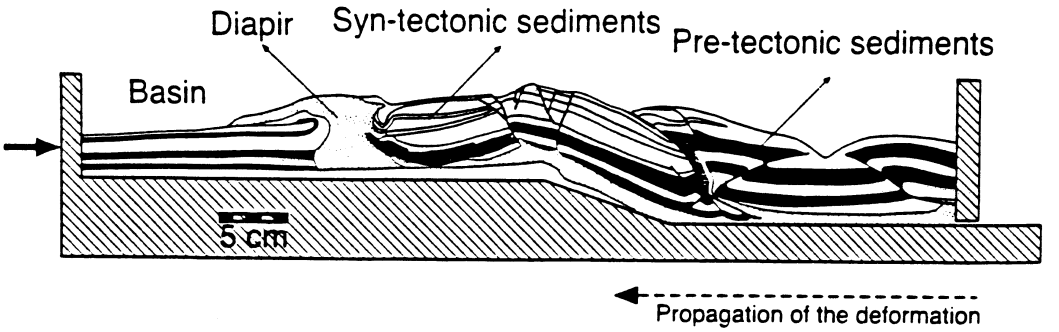

Fig. 12. Sandbox model – final structure redrawn from a cut slice. Compare especially with 'Baena' geological cross-section (Fig. 3). Note that the light grey and white layers in the centre of the structure were added during the diapiric phase of the experiment induced by adding metal weights.

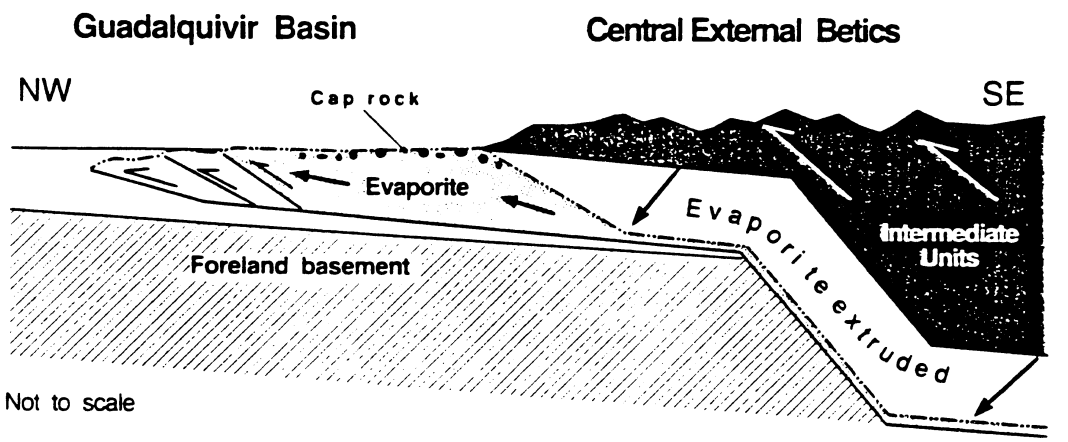

Fig. 13. Schematic model for emplacement of diapiric evaporite–sediment body into the southern margin of the Guadalquivir Basin.

Numerical model

A 2D computer simulation was generated with the aim of improving understanding of the basic mechanisms for lateral diapiric emplacement and to reproduce the early stages of deformation that were not modelled satisfactorilly in the sand-box. The model assumed vertical simple shear deformation along a thrust plane. The hangingwall to this thrust included a Coulomb wedge which corresponds to a thrust sheet stacking piled formely. The footwall consisted of the basement which remained undeformed and which supported an evaporitic basin. For simplicity, we considered only the dynamics of the salt layer rather than using a fully self-consistent dynamic model for the salt and the overburden. The salt layer, which is considered to behave as a viscous newtonian fluid, was overlain by sediments with no strength which deformed in response to the salt-layer dynamics. As the overburden moved with respect to the salt it produced drag of the top of the salt layer. Hence, the numerical approach modelled the response of a thin viscous layer to buoyancy, differential loading and drag forces.

Figure 14 shows the geometric set up considered in this approach which, for consistency, was the same as in the sand-box model. A salt body, of thickness $H(x)$, was acted upon by a pressure $P(x)$ and the salt top was dragged along at a horizontal velocity $u(x)$. The salt body had a density ρ_s and viscosity μ, and the overburden had a density ρ_0. The vertical coordinate y increased upwards from $y = y_0$ at the salt base.

With this set up, and assuming thin film theory, the horizontal salt flux, Q, is given by

$$Q = -(H^3/12\mu)\partial P/\partial x + uH/2. \quad (1)$$

The pressure derivative in equation (1) is controlled by the physical properties of the overburden. Then, for a weak overburden

$$\partial P/\partial x = \rho_0 g\, \partial S/\partial x + (\rho_s - \rho_0)\, g\, \partial H/\partial x \quad (2)$$

where $S(x)$ is the height of the top of the overburden. The first term on the right accounts for differential loading whilst the second term models buoyancy effects. A more complete analysis incorporating the effects of overburden strength and in-plane stresses has been derived in Waltham (1997). Under the assumption of cross-sectional area conservation, the rate of change of salt thickness is given by

$$\partial H/\partial t = -\partial Q/\partial x. \quad (3)$$

Vertical simple shear implies that the hanging-wall horizontal velocities are constant and equal to the compression rate whilst, in the footwall, the horizontal velocities are zero except within the salt body. In addition, the vertical rate of movement, v, within the hanging-wall only depends on x and hence, knowledge of u and $\partial H/\partial t$ allows v to be calculated by (e.g. Waltham & Hardy 1995):

$$\partial H/\partial x = v - u\partial f/\partial x \quad (4)$$

where $f(x,t)$ is the bottom of the overburden or the detachment surface. Once velocities are specified throughout the overburden, any horizon given by $h(x)$ will evolve according to

$$\partial h/\partial t = v - u\partial h/\partial x. \quad (5)$$

Equations (1) to (5) are solved iteratively with time using an explicit finite difference scheme. Boundary conditions allow for flow material associated with the moving overburden through lateral boundaries. The basement remains at rest and undeformed during the process while the top of the model acts as a free surface.

Figure 15 shows the results from the computer model for different time steps and using reasonable values of rate of thrusting, evaporite viscosity, initial evaporite thickness, densities and surface slopes for the study area (Table 2). After 2.5 Ma (Fig. 15a) a thrust, off the right of the model, has generated a Coloumb wedge acting as a differential load on the evaporite. The load affects only the thin part of the evaporite which has therefore not yet moved significantly. After 4.5 Ma (Fig. 15b) the Coloumb wedge has advanced over the thick part of the evaporite and is now producing a diapir ahead of the wedge toe. A new thrust, formed after 5 Ma, detaches in the evaporites and breaks surface off

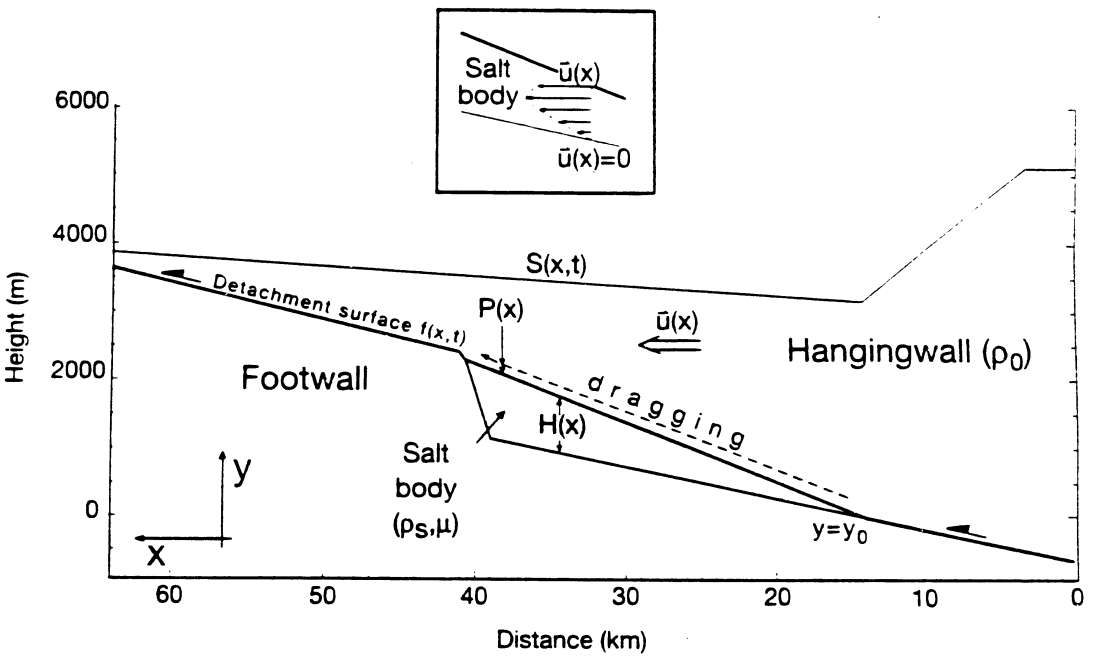

Fig. 14. Geometric set up considered in the numerical model of the salt emplacement. Upper in set: schematic velocity distribution with depth within the salt body. $S(x,t)$ = free surface; $f(x,t)$ = detachment surface, note that this surface change in time.

Table 2. *Computer model parameters*

Coloumb wedge slope	10^{c}
Maximum wedge height	6100 m
Overburden density	2400 kg m^{-3}
Evaporite density	2200 kg m^{-3}
Rate of thrusting	5 m ka^{-1}
Evaporite viscosity	10^{18} Pa s

the left of the model (Fig. 15c). This results in shearing and partial transport leftwards of the evaporite. The final model configuration after 8 Ma is showed in Fig. 15d. Therefore, the differential load on the evaporitic layer associated with the thrusting progression together with the drag from the overburden and buoyancy forces results in the squeezing and further extrussion of the evaporites. These results show that the mechanism proposed for lateral diapiric emplacement is dynamically feasible and matches the main time and spatial features of the evaporite emplacement as observed in the Betics.

The final element of the model is the Coulomb wedge. This is simply imposed as a constant, specified slope which progresses across the model at a specified rate jointly with the overburden. The effect of this is to impose a slowly increasing load on the salt in addition to the load generated by the moving overburden. Note that thin film theory only applies for early stages of salt movement during which concordant (in the sense of Waltham 1997) low amplitude structures are formed. Therefore, the final stages of this process, during which the evaporite diapir breaks through to the surface, has not been modelled numerically. This final process was, however, well reproduced by the physical model.

Discussion

The anomalous chaotic unit in the southern margin of the Guadalquivir Basin was not emplaced as an olistostrome. We interpret this body as emplaced through lateral diapiric processes, partly comparable to those interpreted in the Gulf of Mexico (McGuinness & Hossack 1993). Physical and numerical models can achieve a result that is a good match with the structure of the central Betics as explained and illustrated on Figs 12, 13 and 15.

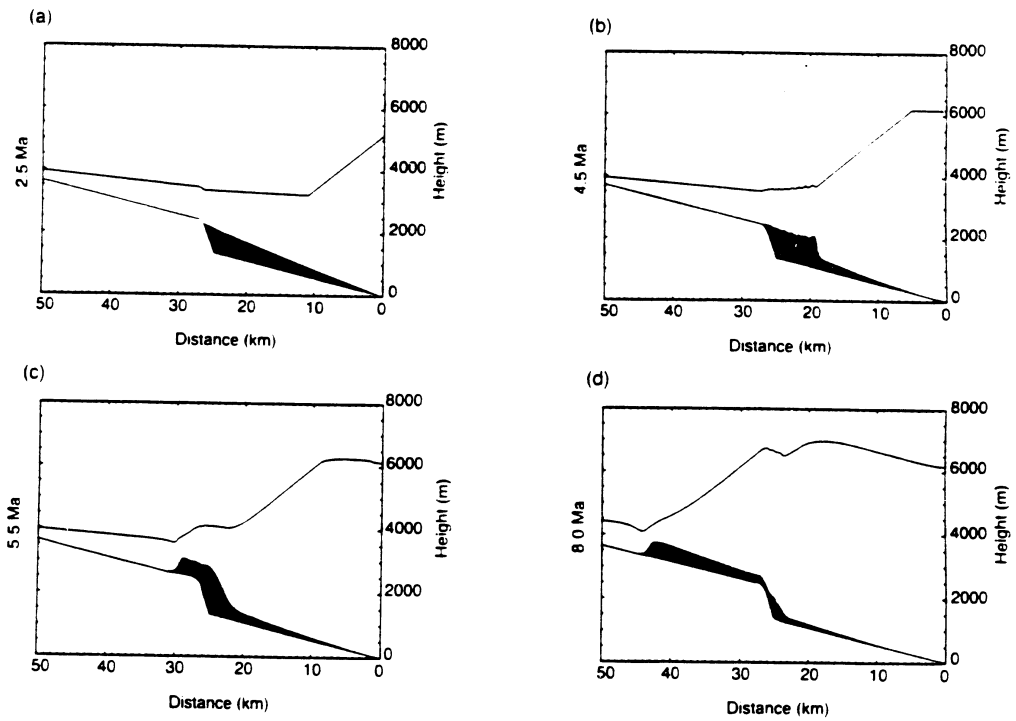

Fig. 15. Numerical modelling results for the evaporite emplacement. (**a**) After 2.5 Ma; (**b**) after 4.5 Ma; (**c**) after 5.5 Ma; (**d**) after 8 Ma. Final model configuration.

In the eastern Betics, evaporites in the Prebetic are responsible for all the diapiric structures (Martínez del Olmo *et al.* 1986; De Ruig 1992). However this evaporite basin dies out some 100 km to the east of the study area. In the central Betics, the Prebetic is much reduced in thickness and extent, and would seem an unlikely place for thick evaporites to have originated (as was concluded by Blankenship 1992 based on 1:200 000 scale geological maps). In the study area, the diapiric Triassic forming the chaotic unit lies immediately north of the Intermediate Units where the Keuper has been tectonically removed, and it seems reasonable to propose that the diapiric body that is now in the Guadalquivir Basin originated in a Triassic basin below the known Jurassic–Cretaceous basin of the Intermediate Unit trough. The approximate northern edge of the original basin is indicated on the 'Martos' cross-section (Fig. 2): its position based on restoration of the small Prebetic thrust slice coincides with the estimated position of the leading edge of the overthrust basement block (admittedly there is little constraint on either of these positions!). Mobile evaporites deposited in such a basin would certainly have become diapirically displaced in some way by loading, first by the Intermediate Units limestones and then, by the denser basement block. If this is the true origin of the material, it implies a lateral displacement of the order of 40 km.

The path along which this expulsion took place, and the mechanism by which the ductile Keuper was pushed ahead of the overlying thrust sheets, is evident from the cross-sections. We consider the most likely expulsion path is above the basal thrust which ramps from the base of ductile Keuper, first to the Prebetic Cretaceous, and then to the Miocene, and below the basal detachment of the Intermediate Units, i.e. at the base of Supra-Keuper. This has become a 'salt weld'. The ductile body could have picked up blocks of Cretaceous and, less easily, Jurassic material by breaking it away from the roof of the diapir as it passed below the hanging-wall cut-off of the Intermediate Units. Any originally coherent-bedded units within the Keuper would have become disrupted as random blocks during this long-distance diapiric transport. The final events of the emplacement are recorded in the most external unit, where sediments originally deposited in the Guadalquivir Basin during Serravallian to Early Tortonian are involved in deformation caused by lateral movement of the diapir, which ceased in Mid-Tortonian times.

Conclusions

(a) The interpretation of geological and geophysical data has allowed us to construct three true-scale, structural cross-sections, which indicates that compression in External Betics was driven by northward emplacement of basement culminations onto a passive continental margin. Compression started probably in the Eocene and propagated through the External Betics during the Miocene, dying out in Tortonian times.

(b) The presence in the central and western Betics of the large chaotic unit composed mainly of Triassic evaporites, emplaced into the southern margin of the Guadalquivir foreland basin, is interpreted as a body extruded from an evaporitic formation originally below the Intermediate Units. It moved by lateral diapiric flow in front of an advancing thrust sheet, and was eventually emplaced as a sea-floor diapir.

(c) Seismic stratigraphy has been used successfully to define sequential arrangement of the sediments filling the basin, and to attribute accurate ages for the emplacement of the diapir. Submarine exposure of the diapir took place initially in the Serravallian, allowing marine sediments of that age to be deposited on top of the Triassic in places, but lateral emplacement of the diapir continued, compressing the basin-floor sediments ahead of it, until at least Mid-Tortonian.

(d) Lateral diapiric emplacement in a compressional setting has been successfully reproduced using both physical and numerical modelling thus demonstrating the plausibility of this process.

(e) From these results, we recommend that this zone should from now on be called the 'Guadalquivir lateral diapir', instead of the word 'olistostrome'. Evaporites are involved in many of the world's thrust belts, and lateral diapirism in some form is probably a widespread phenomenon.

We thank BP Exploration for allowing the use of unpublished data and reports, and J. Hossack for discussions on salt tectonics. B. Colleta and M. Jackson reviews are gratefully acknowledged. We thank M. Keep, M. James and N. Deeks of RHUL's Fault Dynamics Group for providing facilities and assistance in running the sand-box models. Repsol Exploracion supplied seismic profiles and well data. A. Pérez-López and J. Fernandez of Granada University are thanked for useful discussions in the field area. We also thank M. Losantos, for her help in organizing the first manuscript and constructive criticism. This work has been supported financially by the European-Union 'Integrated Basin Studies' project (JOU2-CT92-0110).

References

ALLABY, A. & ALLABY, M. (eds) 1990. *The concise Oxford Dictionary of Earth Sciences*. Oxford University Press, Oxford.

ALLERTON, S., LONERGAN, L., PLATT, J. P., PLATZMAN, E. S. & MCCLELLAND, E. 1993. Palaeomagnetic rotations in the eastern Betic Cordillera, southern Spain. *Earth and Planetary Science Letters*, **119**, 225–241.

BAENA, J. & JEREZ, L. 1982. *Síntesis para un ensayo paleogeográfico entre la Meseta y la Zona Bética s. str.* Colección Informe, I.G.M.E.

BANKS, C. J. & WARBURTON, J. 1991. Mid-crustal detachment in the Betic system of southeast Spain. *Tectonophysics*, **191**, 275–289.

BLANKENSHIP, C. L. 1990. *Structural evolution of the central External Betic Cordillera, southern Spain*. MA Thesis, Rice University, Houston.

—— 1992. Structure and palaeogeography of the External Betic Cordillera, southern Spain. *Marine and Petroleum Geology*, **9**, 256–264.

BLUMENTHAL, M. M. 1927. Versuch einer tektonischen Gliederung der betischen Cordilleren von central und Sudwest Andalusien. *Eclogae Geologicae Helvetiae*, **20**, 487–532.

DE RUIG, M. J. 1992. *Tectono-sedimentary evolution of the Prebetic fold belt of Alicante (SE Spain)*. PhD Thesis, Vrije Universiteit Amsterdam.

FERNANDEZ, M., BERASTEGUI, X., PUIG, C., GARCIA, D., JURADO, M. J., TORNE, M. & BANKS, C. 1998. Geological and geophysical constraints on the evolution of the Guadalquivir Foreland Basin (Spain). *This volume*.

FLETCHER, R. C., HUDEC, M. R. & WATSON, I. A. 1993. Salt glacier model for the emplacement of an allochthonous salt sheet. *In: American Association of Petroleum Geologists, Hedberg Research Conference on Salt Tectonics abstracts*, Bath, UK, 13–17 September 1993.

FONTBOTÉ, J. M. 1965. *Las Cordilleras Béticas. La Depresión del Guadalquivir*. Mapa Geológico de España y Portugal. Nota explicativa. Ed. Paraninfo. Madrid.

—— & VERA, J. A. 1984. La Cordillera Bética. Introducción. *In: Libro Jubilar J.M. Rios, Geologia de España*, **2**. IGME, 343–349.

FRIZON DE LAMOTTE, D., ANDRIEUX, J. & GUÉZOU, J.-C. 1991. Cinématique des chevauchements néogènes dans l'Arc bético-rifain: discussion sur les modèles géodynamiques. *Bulletin de la Société Géologique de France*, **162**, 4, 611–626.

GARCIA-HERNANDEZ, M., LÓPEZ-GARRIDO, A. C., RIVAS, P., SANZ DE GALDEANO, C. & VERA, J. A. 1980. Mesozoic palaeogeographic evolution of the External Zones of the Betic Cordillera. *Geologie en Mijnbouw*, **59**, 155–168.

HAQ, B. U., HARDENBOL, J., VAIL, P. R., AND 10 OTHERS 1987. Mesozoic–Cenozoic Cycle Chart. *In*: BALLY, A. W. (ed.) *Atlas of Seismic Stratigraphy*. American Association of Petroleum Geologists, Studies in Geology, **27**.

HOSSACK, J. R. 1995. Geometrical rules of section balancing for salt structures. *In:* JACKSON, M. P. A., ROBERTS, D. G. & SNELSON, S. (ed.) *Salt tectonics: a global perspective*. AAPG Memoir, **65**, 29–40.

JACKSON, M. P. A. & TALBOT, C. J. 1989. Salt canopies. *In: Gulf Coast Section, Society of Economic Paleontologists and Mineralogists Foundation, 10th Annual Research Conference, Extended Abstracts*, 72–78.

LANAJA, J. M., NAVARRO, A., MARTINEZ ABAD, J. L., DEL VALLE, J., RIOS, L. M., PLAZA, J., DEL POTRO, R. & RODRIGUEZ DE PEDRO, J. 1987. *Contribución de la exploración petrolífera al conocimiento de la geologia de España*. Instituto Geológico y Minero de España, Madrid.

LEBLANC, D. & OLIVER, P. 1984. Role of stike-slip faults in the Betic–Rifian Orogeny. *Tectonophysics*, **101**, 345–355.

MCGUINNESS, D. B. & HOSSACK, J. R. 1993. The development of allochthonous salt sheets as controlled by the rates of extension, sedimentation, and salt supply. *In: Gulf Coast Section of the Society of Economic Paleontologists and Mineralogists Foundation 14th Annual Research Conference*, Extended Abstracts, 127–139.

MARTINEZ DEL OLMO, W., LERET VERDÚ, G. & SUAREZ-ALBA, J. 1986. La estructuración diapírica del Sector Prebético. *Geogaceta*, **1**, 43–44.

MITCHUM, R. M., VAIL, P. R. & THOMSON, S. III. 1977. The depositional sequence as a basic unit for stratigraphic analysis. *In*: PAYTON, C. E. (ed.) *Seismic Stratigraphy. Applications to Hydrocarbon Exploration*. American Association of Petroleum Geologists, Memoirs, **26**, 53–62.

PERCONIG, E. 1960–1962. Sur la constitution geologique de l'Andalousie Occidentale, en particulier du bassin du Guadalquivir (Espagne Meridionale). *In: Livre Mémoire du Professeur Paul Fallot*. Mémoires hors-Série de la Société géologique de France, 229–256.

PÉREZ LÓPEZ, A. D. 1991. *Trias de facies Germánica del sector central de la Cordillera Bética*. PhD Thesis, Univ. Granada.

—— & SANZ DE GALDEANO, C. 1994. Tectónica de los materiales triásicos en el sector central de la Zona Subbética (Cordillera Bética). *Revista de la Sociedad Geológica de España*, **7**, 141–153.

RIAZA, C. & MARTÍNEZ DEL OLMO, W. 1996 Depositional Model of the Guadalquivir- Gulf of Cadiz Tertiary Basin. *In*: FRIEND, P. & DABRIO, C. J. (eds) *Tertiary Basins of Spain: The stratigraphic record of crustal kinematics*. Cambridge University Press, 330–338.

ROLDAN, F. J., LUPIANI, E. & VILLALOBOS, M. 1992. *Cartografía y Memoria de las Hojas Geológicas números 927 (Baeza), 945 (Castro del Rio) y 947 (Jaén) del Mapa Geológico Nacional a Escala 1/50.000*. Instituto Tecnológico Geo-Minero de España, Madrid.

SUAREZ-ALBA, J., MARTÍNEZ DEL OLMO, W., SERRANO OÑATE, A. & LERET VERDU, G. 1989. Estructura del sistema turbidítico de la Formación Arenas del Guadalquivir, Neógeno del Valle del Guadalquivir. *In: Libro Homenaje R. Soler*.

Asociación de Geólogos y Geofísicos Españoles del Petróleo. Madrid. 123–132.

TALBOT, C. J. 1981. Sliding and other deformation mechanisms in a glacier of salt, S. Iran. *In*: MCCLAY, K. R. & PRICE, N. J. (eds). *Thrust and nappe tectonics*. Geological Society, London, Special Publications, **9**, 173–183.

VAIL, P. R. 1987. Seismic stratigraphy interpretation procedure. *In*: BALLY, A. W. (ed.) *Atlas of Seismic Stratigraphy*. American Association of Petroleum Geologists, Studies in Geology, **27**, 1–10.

VAN DER BEEK, P. A. & CLOETINGH, S. 1992. Lithospheric flexure and the tectonic evolution of the Betic Cordilleras (SE Spain). *Tectonophysics*, **203**, 325–344.

VERA, J. A., GARCÍA HERNANDEZ, M., LOPEZ GARRIDO, A. C., COMAS, M. C., RUIZ ORTIZ, P. A. & MARTIN ALGARRA, A. 1982. El Cretácico de las Cordilleras Béticas. *In*: *El Cretácico de España*. Madrid, Universidad Complutense, 515–630.

WALTHAM, D. 1997. Why does salt start to move? *Tectonophysics*, **282**, 117–128.

—— & HARDY, S. 1995. The velocity description of deformation. Paper 1: Theory. *Marine and Petroleum Geology*, **12**, 153–165.